Journal of Power Sources 640 (2025) 236721

Contents lists available at ScienceDirect

Journal of Power Sources

journal homepage: www.elsevier.com/locate/jpowsour

Numerical simulation of lithium dendrite growth in lithium metal batteries: Effect of superimposed AC/DC electric fields on dendrites suppression

Huan Wang [a], Daqian Wang [a], Hao Jiang [b,c], Xiaolei Chen [a], Xiaomin Liu [a,*], Bing Sun [d,**], Yan Wang [a,***]

[a] College of Chemistry and Chemical Engineering, Qingdao University, Qingdao, 266071, China
[b] Beijing Key Laboratory of Ionic Liquids Clean Process, Institute of Process Engineering, Chinese Academy of Sciences, Beijing, 100190, China
[c] School of Chemical Engineering, University of Chinese Academy of Sciences, Beijing, 100049, China
[d] Centre for Clean Energy Technology, School of Mathematical and Physical Sciences, Faculty of Science, University of Technology Sydney, Ultimo, New South Wales, 2007, Australia

HIGHLIGHTS

- Externally superimposed electric fields on mitigating lithium dendrites is proposed.
- A multi-physics field coupling model is established to predict the dendrite growth.
- The mechanism of dendrite inhibition with external field is numerically illustrated.
- The diffusion and migration of lithium ions are critical to dendrite formation.
- Combined application of AC and DC fields effectively optimizes dendrite inhibition.

GRAPHICAL ABSTRACT

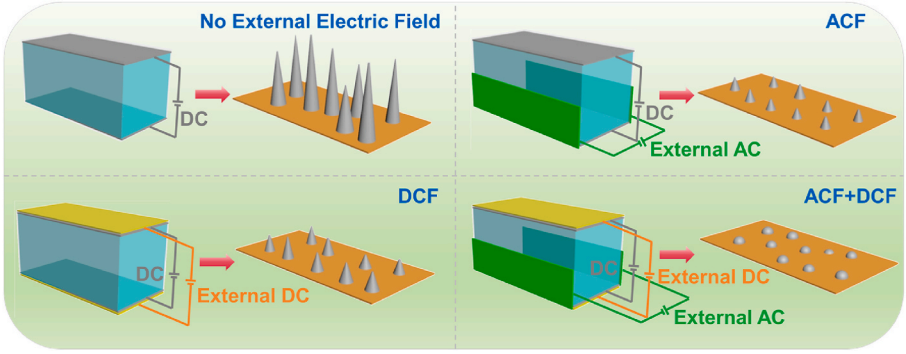

ARTICLE INFO

Keywords:
Lithium metal battery
dendritesuppression
External electric fields
Multi-physics field coupling model
Numerical simulation

ABSTRACT

The employment of external electric fields is a promising strategy for alleviating lithium dendrite formation during lithium metal battery charging. However, the underlying mechanisms that govern dendrite formation remain unclear. Herein, we present numerical insights into the impact of externally superimposed alternating current (AC) and direct current (DC) electric fields on the suppression of lithium dendrite formation in lithium metal batteries. A theoretical model by coupling the phase field, electric field and ion concentration field is established to predict lithium dendrite growth. Numerical investigations are carried out to understand the fundamental mechanisms of dendrite formation and inhibition in the presence of external AC/DC electric fields. External AC/DC fields applied perpendicular to the internal field enhance Li-ion diffusion by distorting electric field distribution, thereby reducing concentration gradients and local current densities near the anode surface. Similarly, AC/DC fields aligned parallel to the internal field promote uniform lithium deposition by accelerating Li-ion migration and diffusion through an intensified electric field. Consequently, the simultaneous

* Corresponding author.
** Corresponding author.
*** Corresponding author.
E-mail addresses: liuxiaomin@qdu.edu.cn (X. Liu), bing.sun@uts.edu.au (B. Sun), yanwang@qdu.edu.cn (Y. Wang).

https://doi.org/10.1016/j.jpowsour.2025.236721
Received 9 January 2025; Received in revised form 18 February 2025; Accepted 3 March 2025
Available online 7 March 2025

superimposition of AC and DC fields demonstrates an optimal dendrite inhibition effect, reducing the dendrite area to 14.01 % compared to conditions without external fields. This work offers a theoretical basis for lithium dendrite suppression via superimposed electric fields.

1. Introduction

Aiming at the rapid global transition to renewable energy and electrification, the demand for high-energy-density power batteries has become increasingly urgent [1–3]. Li-ion batteries with graphite anodes have nearly reached their theoretical energy density limits [4–6]. Next-generation anode materials such as lithium metal are regarded as ideal alternatives to graphite anodes due to its exceptionally high theoretical specific capacity and low electrochemical potential [7–10]. Although lithium metal batteries (LMBs) hold significant promise, they still face considerable challenges, including detrimental effects of unstable solid electrolyte interfaces (SEI) on cycle life [11–13] and safety risks related to lithium dendrite growth [14–16].

To mitigate challenges associated with lithium dendrite formation, researchers have explored a range of strategies, such as the use of electrolyte additives [17–19], surface modifications of electrodes [20–22] and the incorporation of solid electrolytes [23–25]. However, these methods mainly concentrate on internal modifications of batteries and frequently encounter issues during long-term usage. For instance, electrolyte additives have the risk of degradation or adverse reactions during cycling [26–28], while modification layers on electrodes often suffer from deterioration, malfunction or exfoliation during repeated charge-discharge cycles [29,30]. Additionally, solid electrolytes may experience mechanical stress and undergo volumetric changes over time [31–33]. Consequently, exploring external environmental optimization strategies, distinct from conventional internal modifications, holds significant research importance.

Recent evidence demonstrates that the employment of external fields such as magnetic, stress, and electric fields can effectively restrain the growth of lithium dendrites [34,35]. For example, the application of a magnetic field induces magnetohydrodynamic (MHD) effects within the battery, causing Li-ions to move in a spiral trajectory under the influence of the Lorentz force. The alteration in the deposition rate and pattern of Li-ions in the presence of the external magnetic field promotes more uniform deposition, thereby minimizing dendrite formation. Shen et al. [36] applied a nickel-cobalt (NiCo) alloy coating onto the three-dimensional (3D) copper foam to function as the current collector. Through numerical simulations and in-situ observations, it was demonstrated that the spiral motion of Li-ions, in conjunction with MHD effects under applied magnetic fields, can mitigate the growth of lithium dendrites and facilitate the formation of compact Li deposits. However, the inhibition mechanism exerted by an applied magnetic field on lithium dendrites formation is relatively complex, involving multiple factors such as MHD and alterations in the trajectory of Li-ions. Moreover, these mechanisms may differ across various battery systems and experimental conditions. In contrast, the inhibition mechanism of an externally applied electric field on lithium dendrites is more direct and distinct, which is primarily achieved through influencing the migration and deposition behaviors of Li-ions. The application of electric fields supplies an additional driving force for Li-ion migration, directing the ions to move along the field lines and modifying their deposition behavior on the electrode. This electric field fosters a more uniform distribution of Li-ions on the electrode surface, thus mitigating dendrite growth. A pioneering investigation into electric field-based inhibition of dendrite growth was conducted by Han et al. [37], who applied an alternating current (AC) electric field perpendicular to the anode in conjunction with a direct current (DC) electric field. They experimentally demonstrated the proposed dual-field approach effectively enhanced Li-ion transport within the electrolyte and reduced the concentration gradient near the anode, thereby successfully inhibiting dendrite formation. While experimental evidence demonstrates the effectiveness of electric fields, the utilization of external electric fields to suppress dendrite growth in lithium metal batteries requires further validation through theoretical modelling and numerical simulations, as current theoretical support remains insufficient. In fact, recent studies have shown that the phase-field method can be used to describe lithium dendrite growth behavior through modeling and simulations [38–40]. For example, Qi et al. [41] constructed a three-dimensional multi-physical-field coupled phase-field model based on the principle of free energy minimization. They utilized the finite element method to solve the developed model via the COMSOL software, simulating the growth of lithium dendrites with various morphologies. Subsequently, they numerically analyzed the influences of factors such as anisotropy and temperature and proposed a method for stabilizing lithium deposition based on the internal potential analysis of multi-nuclear lithium dendrites. Evidently, the feasibility of using the phase-field method to simulate dendrite growth has been fully verified.

Herein, we present a numerical investigation into the impact of superimposed AC/DC electric fields on the suppression of lithium dendrite formation. A theoretical model by coupling phase field, ion concentration field and electric field is established to predict the lithium dendrite process in lithium metal batteries. Based on the proposed model, the mechanisms of lithium dendrite growth in the presence of external AC/DC electric fields are for the first time elucidated via numerical simulations. Besides, the impact of field factors such as the applied voltage, frequency, and the direction of external electric fields on dendrite growth and morphology is investigated. This work is anticipated to offer theoretical support for the application of external electric fields in suppressing dendrite formation in lithium metal batteries.

2. Numerical modelling

2.1. Phase field model

In the phase field model, the electrochemical reaction involved in lithium insertion and extraction in lithium metal batteries is given by:

$$Li^{+} + e^{-} \leftrightarrow Li \tag{1}$$

In electrodeposition systems, the expression for Gibbs free energy is presented as follows [40,42,43]:

$$G = \int_{V} \left[f_{\mathrm{ch}}(\xi, c) + f_{\mathrm{grad}}(\nabla \widetilde{c}) + f_{\mathrm{elec}}(c, \varphi) \right] dV \tag{2}$$

where $f_{\mathrm{ch}}(\xi, c)$ is the Helmholtz free energy density, $f_{\mathrm{grad}}(\nabla \widetilde{c})$ is the gradient energy density, and $f_{\mathrm{elec}}(c, \varphi)$ is the electrostatic energy density, given as:

$$f_{\mathrm{ch}}(\xi, c) = \mathrm{g}(\xi) + c_0 RT(\widetilde{c}_{+} \ln \widetilde{c}_{+} + \widetilde{c}_{-} \ln \widetilde{c}_{-}) + \sum c\mu^{\vartheta} \tag{3}$$

$$f_{\mathrm{grad}}(\nabla \widetilde{c}) = \frac{1}{2} \nabla \widetilde{c} \bullet \kappa(\theta) \nabla \widetilde{c} \tag{4}$$

$$f_{\mathrm{elec}}(c, \varphi) = \rho_{\mathrm{c}} \varphi \tag{5}$$

where $c = \{c, c_{+}, c_{-}\}$ are the concentrations of Li atoms, Li^{+} cations and PF_6^{-} anions, respectively. $\widetilde{c} = \{\widetilde{c} = c/c_{\mathrm{s}}, \widetilde{c}_{+} = c_{+}/c_0, \widetilde{c}_{-} = c_{-}/c_0\}$ is the dimensionless concentrations. ξ is the phase field order parameter($\xi = 1$ denotes metallic lithium, $\xi = 0$ denotes electrolyte, $0 < \xi < 1$ denotes interface). c_{s} is the density of metallic lithium; c_0 is the initial concen-

tration of the electrolyte. μ^{ϑ} is the standard chemical potential. $\kappa(\theta) = \kappa_0(1+\delta\cos(\omega\theta))^2$ is the gradient coefficient; κ_0 is the gradient energy coefficient; δ is the anisotropy strength; ω is the anisotropy modulus (set to 4); θ is the angle between the interface normal and the reference axis. ρ_c is the charge density; φ is the electrostatic potential; V is the volume.

The electrochemical reaction rate can be expressed by using the Butler-Volmer equation, as follows [44–46]:

$$R_e = -R_0\left\{exp\left[\frac{(1-\alpha)nF\eta}{RT}\right] - exp\left[\frac{-\alpha nF\eta}{RT}\right]\right\} \tag{6}$$

where R_0 is the exchange current density ; $1-\alpha$ and α are the charge transfer coefficients for the anode and cathode, respectively. η is the activation overpotential; n is the number of electrons involved in the reaction. F, R, T are the Faraday constant, the universal gas constant and the temperature, respectively.

The partial differential equation governing the time evolution of the phase field variable can be derived in conjunction with the Butler-Volmer equation, as follows [43,47,48]:

$$\begin{aligned}\frac{\partial\xi}{\partial t} = &-L_\sigma\left[g'(\xi) - \nabla\bullet(\kappa(\theta)\nabla\xi) + \frac{1}{2}\frac{\partial}{\partial x}\left(\kappa'(\theta)\frac{\partial\xi}{\partial y}\right) - \frac{1}{2}\frac{\partial}{\partial y}\left(\kappa'(\theta)\frac{\partial\xi}{\partial x}\right)\right]\\ &-L_\eta h'(\xi)\left[exp\left(\frac{(1-\alpha)nF\eta}{RT}\right) - \widetilde{c}_+\, exp\left(\frac{-\alpha nF\eta}{RT}\right)\right]\end{aligned} \tag{7}$$

where L_σ is the interface mobility; L_η is the reaction constant. $g(\xi) = W\xi^2(1-\xi)^2$ is a double-well function used to distinguish between the electrolyte $(\xi = 0)$ and metallic lithium $(\xi = 1)$; W is the height of the potential barrier. $h(\xi) = \xi^3(6\xi^2 - 15\xi + 10)$ is an interpolation function varying from 0 to 1, designed to ensure that the electrochemical reaction is confined to the deposition-electrolyte interface.

The partial differential equation describing the time evolution of the Li-ion concentration can be expressed by using the continuity equation and the Nernst-Planck equation, as follows [43,44,48]:

$$\frac{\partial\widetilde{c}_+}{\partial t} = \nabla\bullet\left(D^{eff}\nabla\widetilde{c}_+ + D^{eff}\frac{\widetilde{c}_+ nF}{RT}\nabla\varphi\right) - \frac{c_s}{c_0}\frac{\partial\xi}{\partial t} \tag{8}$$

where $D^{eff} = D^e h(\xi) + D^s(1-h(\xi))$ is the effective diffusion coefficient; D^e and D^s are the diffusion coefficients of Li-ions in the electrode and electrolyte, respectively.

The distribution of the electrostatic potential is described using the Poisson equation, as follows [43,44]:

$$\nabla\bullet\left[\sigma^{eff}\nabla\varphi\right] = I_R = nFc_s\frac{\partial\xi}{\partial t} \tag{9}$$

where $\sigma^{eff} = \sigma^e h(\xi) + \sigma^s(1-h(\xi))$ is the effective electrical conductivity, σ^e and σ^s are the electrical conductivities of the electrode and the electrolyte, respectively.

2.2. Design principles

Without the application of an external electric field, lithium metal batteries often undergo pronounced lithium dendrite formation on the anode surface during rapid charging (Fig. 1a). To address this issue, an alternating current field (ACF) applied perpendicularly to the internal electric field direction is proposed in this study. The ACF guides Li-ions to move along a specific path on the anode surface, promoting uniform Li-ion flux distribution and considerably inhibiting dendrite growth (Fig. 1b). Additionally, a direct current field (DCF) aligned with the internal electric field direction is examined. The DCF provides an additional driving force for Li-ion migration, accelerating their movement along the field lines and promoting homogeneous lithium deposition, thereby effectively restraining dendrite formation (Fig. 1c). Ultimately, by superimposing both ACF and DCF, the lithium dendrite growth issue is expected to be minimized (Fig. 1d). For the combined approach presented in Fig. 1d, the DCF drives Li-ions towards the anode surface, while the ACF facilitates their movement along the surface. The synergistic effect of both fields can ensure a more rapid and uniform distributions of Li-ions on the electrode surface, thus significantly preventing dendrites formation.

2.3. Boundary conditions and initial values

In this study, the general form PDE module in COMSOL Multiphysics 6.2 is utilized for numerical simulations. The computational domain encompasses a square area of $6 \times 6\ \mu m^2$ square area, with three initial nucleation sites represented by a semi-elliptical shape positioned at the lower boundary of the domain. The growth of lithium dendrites is predominantly governed by physical processes occurring in the vicinity of the electrode surface, such as Li-ion diffusion and electric field distribution. While certain factors in 3D space may influence dendrite formation, two-dimensional (2D) simulations in the preliminary research phase can adequately capture the principal physical phenomena and serve as a crucial reference for elucidating the underlying growth mechanisms [38,49]. Hence, the model can be simplified to a 2D computational domain (Fig. 2). For the phase field, Neumann boundary conditions with a value of 0 are applied to all four boundaries of the model. For the ion concentration field, the upper boundary is assigned with Dirichlet boundary conditions at c_0, while the remaining three boundaries utilize Neumann boundary conditions with a value of 0. For the electric potential field, the upper boundary is assigned Dirichlet boundary conditions at 0.1 V, and the other three boundaries are subject to Neumann boundary conditions with a value of 0. To apply the DCF or ACF parallel to the internal electric field direction, the field is directly exerted along the vertical direction of the electric potential field. Conversely, to apply the DCF or ACF perpendicular to the anode surface, Dirichlet boundary conditions are set at the left and right boundaries of the model, with values of $-\varphi/2$ and $\varphi/2$ respectively. All relevant simulation parameters are detailed in Table 1.

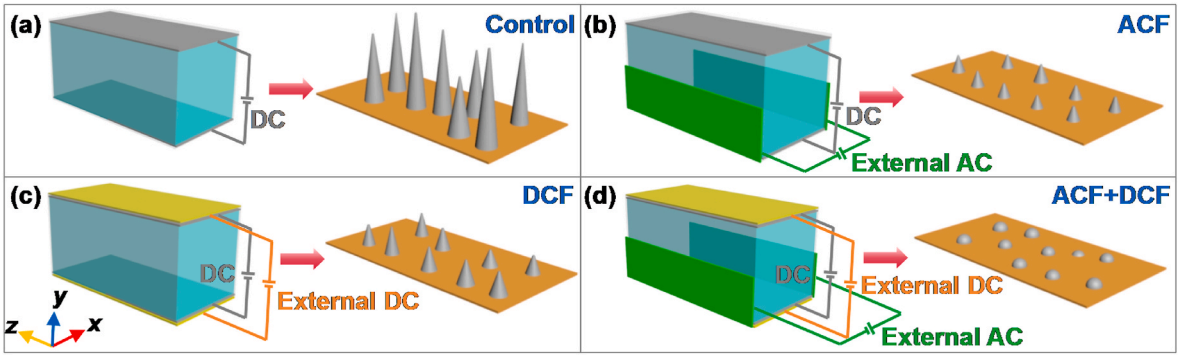

Fig. 1. Schematic of lithium dendrite growth: (a) No external electric field; (b) External ACF; (c) External DCF; (d) Combined ACF and DCF.

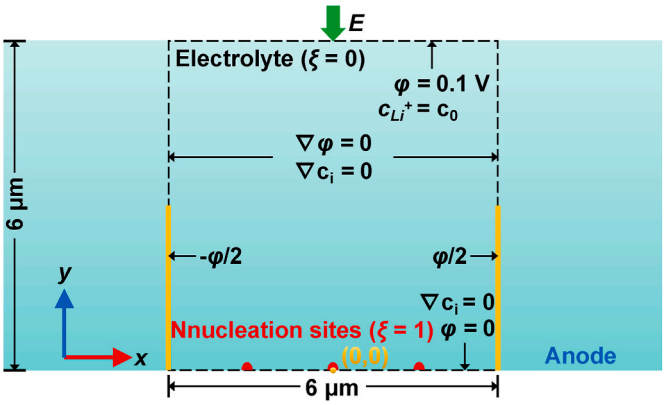

Fig. 2. Computational domain and boundary conditions for numerical simulations.

Table 1
All relevant parameters used for the simulation.

Symbol	Parameter	Value	Unit	Ref.
L_σ	Interfacial mobility	1.0×10^{-6}	$m^3\ J^{-1}\ s^{-1}$	[50]
L_η	Reaction constant	0.5	s^{-1}	[50]
W	Barrier height	3.5×10^5	$J\ m^{-3}$	[50]
σ^e	Conductivities of electrode	1.0×10^7	$S\ m^{-1}$	[45, 50]
σ^s	Conductivities of electrolyte	0.1	$S\ m^{-1}$	[50]
α	Charge transfer coefficient	0.5	1	[50, 51]
c_0	Li-ions bulk concentration	1.0×10^3	$mol\ m^{-3}$	[50, 52]
c_s	Site density of Li metal	7.69×10^4	$mol\ m^{-3}$	[50]
D^e	Diffusion coefficient in electrode	2.0×10^{-16}	$m^2\ s^{-1}$	[50]
D^s	Diffusion coefficient in electrolyte	2.0×10^{-15}	$m^2\ s^{-1}$	[50]
κ_0	Gradient energy coefficient	1.0×10^{-10}	$J\ m^{-1}$	[50]
δ	Anisotropy	0.2	1	–
F	Faraday's constant	96485	$C\ mol^{-1}$	[39, 50]
R	Ideal gas constant	8.314	$J\ mol^{-1}\ K^{-1}$	[39, 50]
T	Temperature	298.15	K	[49]

2.4. Model and mesh independence verification

The model utilized in this study was verified by comparing the numerical simulations of the field distributions with the literature values presented by Han et al. [50]. As illustrated in Fig. S1, the simulated phase field and electric field display a substantial degree of concordance with those documented in the literature, thus manifesting the outstanding accuracy of the proposed model. To ensure that the simulation results are independent of the mesh size, a mesh independence verification was performed (see Fig. S2). The relative deviations of the simulated phase field distribution between various selected mesh numbers (55,485, 89,787, 121,203, and 174,243) and the finest mesh number (217083) were determined to be 18.05 %, 8.82 %, 8.76 %, and 4.83 %, respectively. To balance data accuracy and computational efficiency, a total mesh count of 174,243 was selected for all numerical simulations.

3. Results and discussion

3.1. Field distributions of the applied ACF/DCF perpendicular to internal electric field direction

Fig. 3a, e and 3i illustrate the morphology of lithium dendrites at 5 s in the absence of an external electric field, as well as with ACF or DCF applied perpendicular to the internal electric field direction. It is evident that the area occupied by dendrites reduces significantly the presence of external electric fields. Both ACF and DCF demonstrate substantial suppression effects on dendrite growth, with ACF yielding the smallest dendrite area, indicating the most effective suppression. In conjunction with the quantitative statistics of the dendrite region presented in Fig. 4a, it is evident that, at the same time point, the dendrite area is markedly reduced when ACF or DCF is applied perpendicular to the internal electric field direction, with ACF demonstrating the most substantial effect. The disparity in dendrite area among these conditions increases over time (see Fig. S3), suggesting that the suppression effect becomes increasingly apparent as time progresses.

Fig. 3b, f and 3j illustrate the corresponding distributions of Li-ion concentration. The color bands surrounding dendrites subjected to ACF or DCF are significantly broader than those without an applied field, indicating a reduced concentration gradient. As depicted in Fig. 4b, the application of ACF minimizes the concentration gradient in the y-direction, facilitating more uniform Li-ion deposition and consequently inhibiting dendrite growth.

Fig. 3c, g and 3k present the corresponding electric potential distributions, where application of ACF or DCF results in a higher degree of non-uniformity in the y-direction. As shown in Fig. 4c, the potential gradient in the y-direction is apparently higher in the presence of either ACF or DCF compared to the case without the external electric field, indicating a greater field variation and hence a stronger electric force exerted on Li-ions. As depicted in Fig. 4e, in the absence of an external electric field, Li-ions migrate toward the anode surface in alignment with the direction of the internal electric field. However, when the migration rate of Li-ions does not correspond to the reaction rate, the local concentration of Li-ion becomes excessively high, resulting in the formation of a concentration gradient. This gradient compels Li-ions to preferentially deposit in regions of higher concentration, thereby initiating dendrite growth. By applying an external ACF, a potential difference is established between the upper boundary and the left and right boundaries, which alters the distribution of electric field lines along both sides (as illustrated in Fig. S4). It can be anticipated that Li-ions will migrate along the potential lines toward both sides, which enhances their diffusion rate and mitigates the concentration gradient resulting from decreased local Li-ion concentrations, thus suppressing dendrite growth.

Fig. 3d, h and 3l present the corresponding current density distributions. The brown region observed on the left side of ACF/DCF model is ascribed to the negative potential applied at the left boundary. In the absence of an external electric field, a relatively high current density is observed at the dendrite tips, which facilitates their growth in the y-direction. However, upon the application of ACF or DCF, the current density becomes more uniform. This results in a relatively high current density on both lateral sides of the dendrite, promoting its growth in the x-direction. Fig. 4d further reveals a highly uneven current density distribution in the y-direction in the absence of an external electric field. In contrast, the application of ACF or DCF reduces local current density, leading to a more uniform lithium deposition layer, which subsequently suppresses dendrite growth in the y-direction. Similarly, in the x-direction, the presence of an external electric field results in a comparatively uniform current density, facilitating the dendrites to grow evenly towards the left and right sides, thereby indirectly suppressing dendrite growth in the y-direction (Fig. 4f).

As demonstrated above, a better suppression effect of dendrite growth is achieved by applying ACF perpendicular to the internal

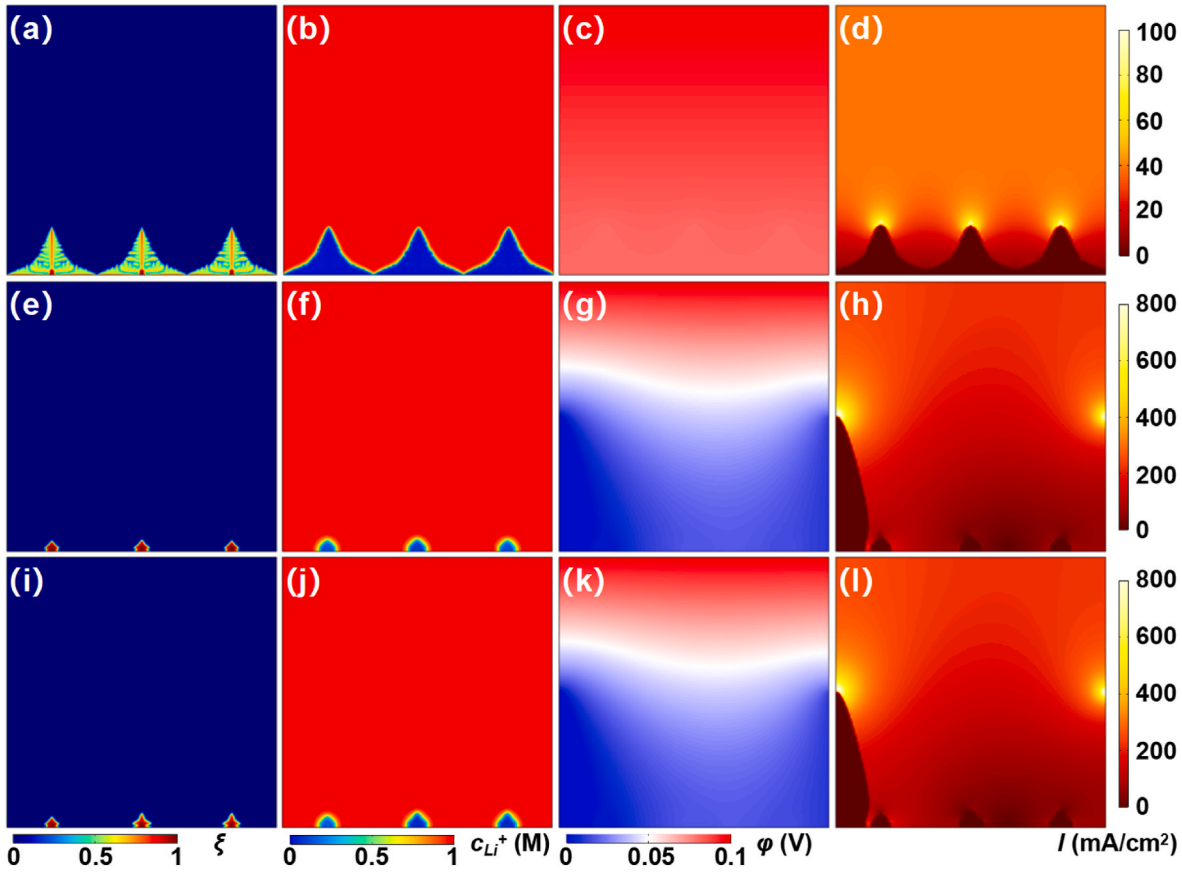

Fig. 3. Effects of no external electric field and applying ACF (0.02 V, 25 Hz) or DCF (0.02 V) perpendicular to the internal electric field direction on lithium dendrites: (a, e, i) Morphology of lithium dendrites; (b, f, j) Li-ion concentration distribution; (c, g, k) Electric potential distribution; (d, h, l) Current density distribution.

electric field direction. This prompted further investigation into the influence of varying AC voltages and field frequencies on dendrite formation. The ratio of dendrite area with ACF to that without external electric field decreases with reducing AC voltage, indicating that lower AC voltages suppress dendrite growth more effectively (Fig. 4g). This is likely due to the enhanced precision in controlling the distribution and deposition behavior of Li-ions at lower voltages. The optimal suppression effect is observed at an input voltage of 0.02 V. Further reduction in voltage does not significantly improve the dendrite suppression. Therefore, considering both performance and energy consumption, 0.02 V is identified as the optimal AC voltage for lithium dendrite inhibition. Fig. 4h presents the suppression of dendrite growth across different AC frequencies. At an AC frequency of 25 Hz, the dendrite suppression effect is marginally superior to that at zero frequency (corresponding to DCF), demonstrating a dendrite area that is only 15.75 % of the area observed without an external electric field. The increase in frequency (from 25 to 200 Hz) does not significantly alter the dendrite area ratio, likely because the ACF effect arises from the potentials applied at the left and right boundaries, which maintain a consistent electric field direction over time. The potential difference between these boundaries and the top boundary causes the electric field to consistently distribute from top to side, with little variation in its direction. Consequently, the field frequency has minimal influence on dendrite growth, thus the 25 Hz is selected as an optimal AC frequency.

3.2. Field distributions of the applied ACF/DCF parallel to internal electric field direction

The lithium dendrite morphology under three conditions, i.e., without an external electric field, applying ACF (0.05 V, 25 Hz) parallel to the internal electric field, and applying DCF (0.05 V) parallel to the internal electric field, is presented in Fig. 5a, e and 5i, respectively. It can be observed that under ACF, the dendrites transform from sharp, elongated tree-like structures to smooth and spherical forms. In contrast, dendrite growth under DCF slows down significantly, resulting in a more regular and compact structure. Quantitative dendrite morphology analysis reveals that, at the same time point, the dendrite area is smallest when DCF is applied parallel to the internal electric field, followed by ACF, with the largest area occurring in the absence of an external electric field (Fig. 6a). This indicates that both ACF and DCF can effectively suppress dendrite growth when aligned with the internal electric field, with DCF exhibiting greater efficacy. The difference in dendrite area becomes more pronounced over time (see Fig. S5), and the suppression effect becomes increasingly significant.

The concentration distribution of Li-ion shown in Fig. 5b, f and 5j resembles the dendrite morphology, with apparent concentration gradients observed at the dendrite growth boundaries. From the electric potential distributions presented Fig. 5c, g and 5k, it is evident that the potential is most uniform without an external electric field, while the application of DCF results in the most uneven potential distribution. According to Fig. 6b, the potential profile exhibits the steepest slope, indicating the largest potential gradient in the y-direction. This corresponds to the highest electric field strength and hence the strongest electric acting force on Li-ions. We thus infer from the results that applying DCF parallel to the internal electric field effectively suppresses dendrite growth. This is primarily because the internal electric field aligns with the DCF, increasing the overall electric field strength (Fig. S6). This enhancement accelerates Li-ions diffusion within the electrolyte, promotes a more uniform distribution on the anode surface, and prevents localized depletion of Li-ions. Consequently, the reaction

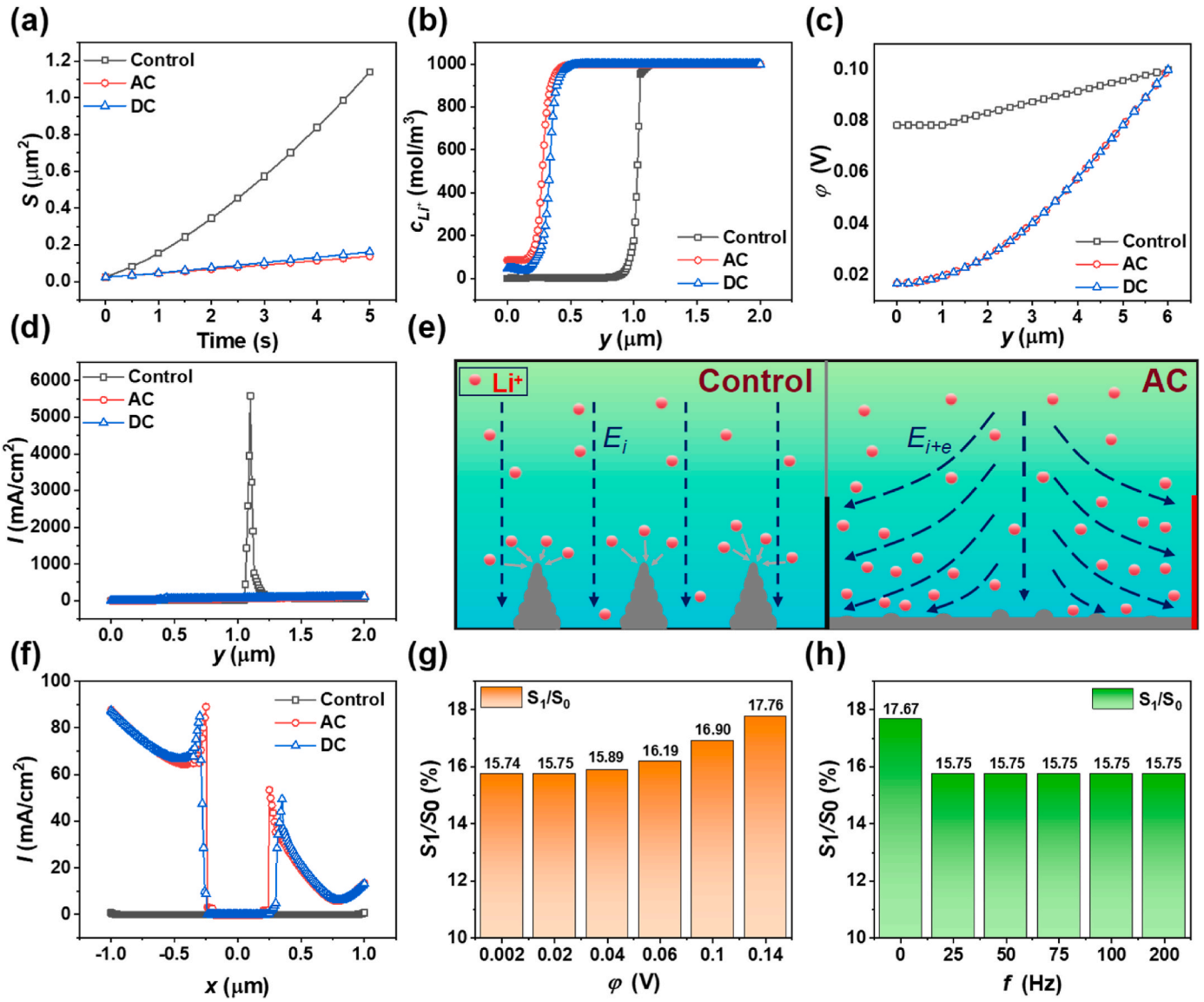

Fig. 4. (a) Variation of dendrite area over time; (b) Li-ion concentration distribution in the y-direction(x = 0,0≤y ≤ 2); (c) Potential distribution in the y-direction(x = 0,0≤y ≤ 6); (d) Current density distribution in the y-direction(x = 0,0≤y ≤ 2); (e) Schematic of dendrite suppression effect with ACF applied perpendicular to the internal electric field (E_i is the internal electric field, E_{i+e} represents the combination of internal electric field and external electric field); (f) Current density distribution in the x-direction(-1≤x ≤ 1,y = 0.1); (g) Ratio of dendrite area with ACF applied (S_1) to that without external electric field (S_0) at different AC voltages; (h) S_1/S_0 at different AC frequencies.

rate increases with external DCF, resulting in more uniform deposition and further inhibiting dendrite formation and growth (Fig. 6d) [37]. In contrast, ACF with varying electric field direction only intermittently enhances the electric field strength, making it less effective at suppressing dendrite growth compared to DCF. Fig. 5d, h and 5l present the corresponding current density distributions. Due to the high current density at the dendrite tips, the transport rate of Li-ions on the electrode surface is insufficient to meet the demand of the electrochemical reaction, leading to Li-ions accumulation at the protruding regions and thereby promoting dendrite growth. Fig. 6c further demonstrates a high degree of unevenness in the current density in the y-direction without an external electric field. However, by applying ACF or DCF, the reduction in local current density promotes the formation of a more uniform lithium deposition layer, which in turn suppresses dendrite growth in the y-direction.

The above results demonstrate the most effective suppression of lithium dendrite growth is accomplished by applying DCF parallel to the internal electric field. As shown in Fig. 6e, the ratio of dendrite area with DCF decreases with the increasing of DC voltage at low applied voltages. However, when the voltage reaches 0.1 V, further increases in voltage beyond 0.1 V do not significantly enhance the suppression of dendrites. This is mainly because, at 0.1 V, the diffusion rate of Li-ions closely aligns with the reaction rate, and additional voltage only maintains the diffusion rate without further improvement due to the reaction rate limitations. As such, an external DCF with 0.1 V is identified as the optimal voltage.

3.3. *Parametric study of superimposed ACF and DCF on lithium dendrite suppression*

Given the effectiveness of ACF and DCF in suppressing lithium dendrite growth, we further explored the combined application of both electric fields. By comparing the dendrite morphology under the optimal conditions for ACF (0.02 V, 25 Hz) and DCF (0.1 V) with that observed without any applied electric field, we found that the combined electric field significantly inhibits dendrite growth, as shown in Fig. S7.

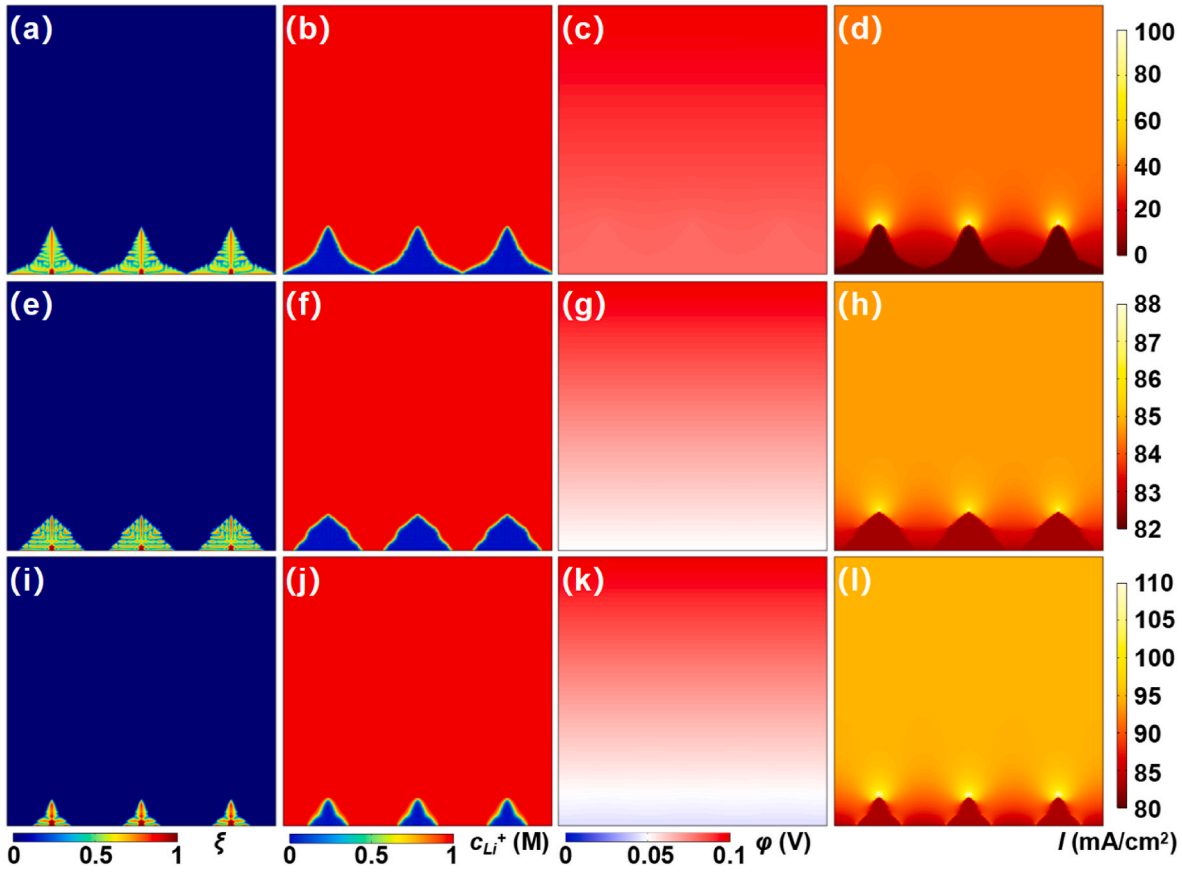

Fig. 5. Effects of no external electric field and applying ACF (0.05 V, 25 Hz) or DCF (0.05 V) parallel to the internal electric field direction on lithium dendrites: (a, e, i) Morphology of lithium dendrites; (b, f, j) Li-ion concentration distribution; (c, g, k) Electric potential distribution; (d, h, l) Current density distribution.

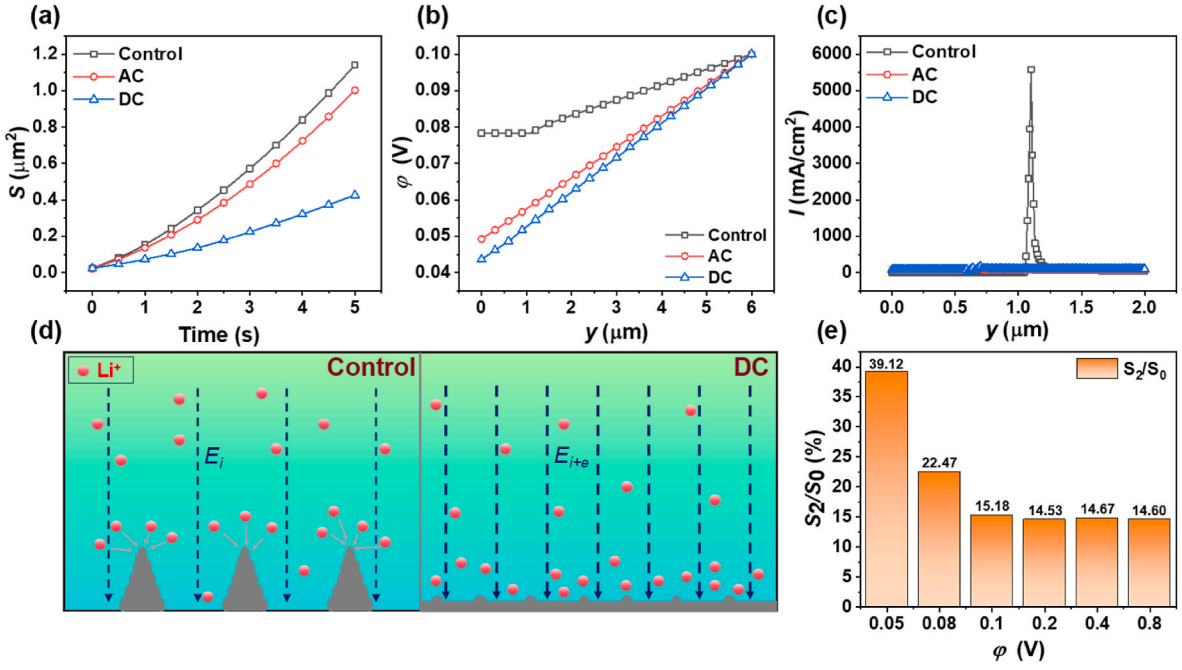

Fig. 6. (a) Variation in lithium dendrite area with time; (b) Potential distribution in the y-direction (x = 0, 0≤y ≤ 6); (c) Current density distribution in the y-direction (x = 0, 0≤y ≤ 2); (d) Schematic of dendrite suppression by applying DCF parallel to the internal electric field; (e) Effect of different DC voltages on lithium dendrites: Ratio of dendrite area with DCF (S_2) to dendrite area without applied electric field (S_0).

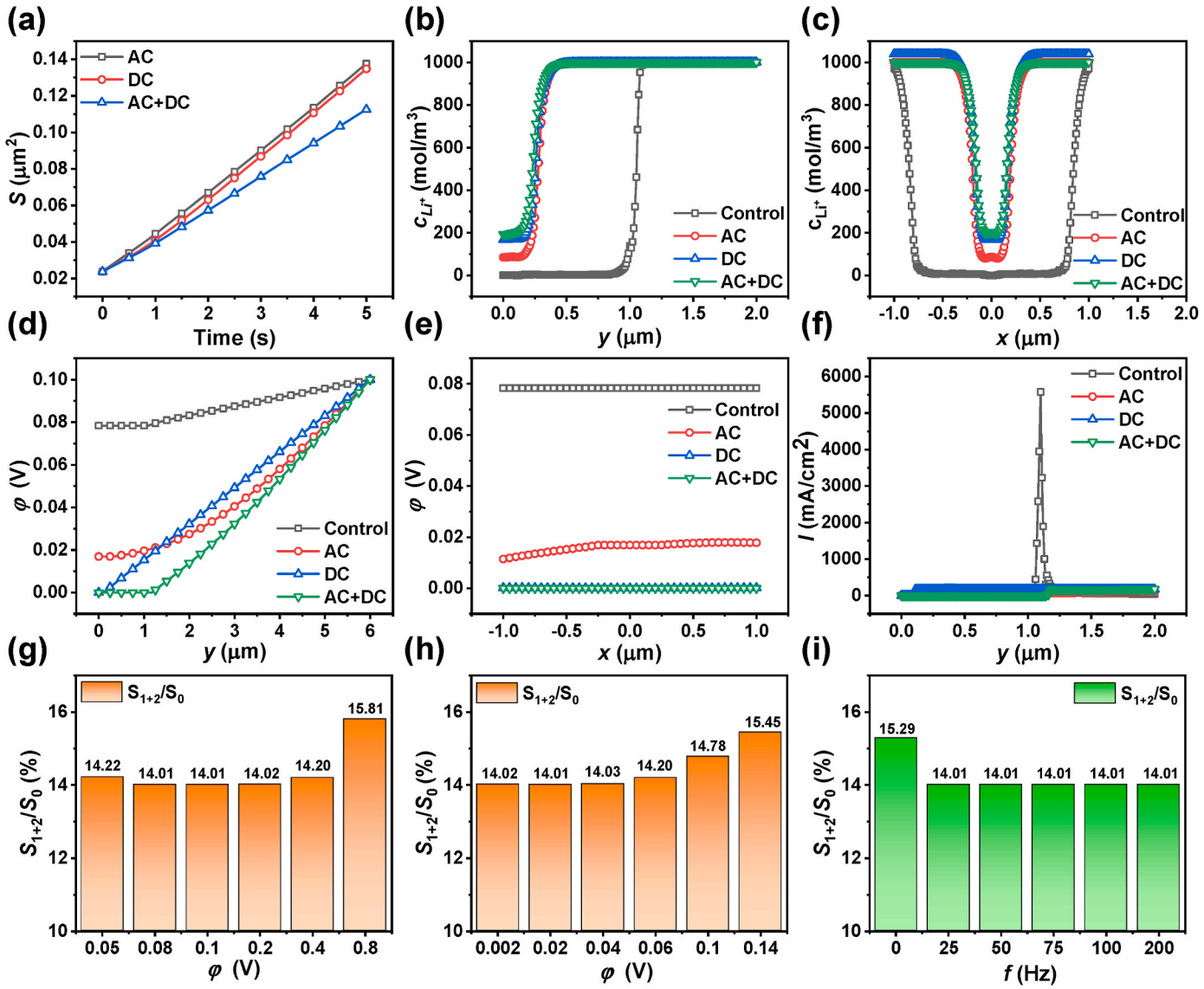

Fig. 7. (a) Variation of dendrite area with time; (b) Li-ion concentration distribution in the y-direction (x = 0, 0≤y ≤ 2); (c) Li-ion concentration distribution in the x-direction (−1≤x ≤ 1, y = 0.1); (d) Electric potential distribution in the y-direction (x = 0, 0≤y ≤ 6); (e) Electric potential distribution in the x-direction (−1≤x ≤ 1, y = 0.1); (f) Current density distribution in the y-direction (x = 0, 0≤y ≤ 2); Ratio of dendrite area with ACF + DCF (S_{1+2}) to the dendrite area without an applied electric field (S_0); (g) Effect of different DC voltages; (h) Effect of different AC voltages; (i) Effect of different AC frequencies.

Additionally, the suppression effects of the combined were compared to those of ACF and DCF individually. As shown in Fig. 7a, the dendrite area under the combined ACF and DCF field is markedly smaller than that under either ACF or DCF alone, indicating that the combined field is more effective in suppressing lithium dendrite growth than the individual fields. Fig. 7b and c presents the distributions of Li-ion concentration in the y-direction and x-direction, respectively. The combined electric field results in the smallest concentration gradients in both directions, suggesting that it reduces the concentration gradients effectively in both directions, thereby providing superior inhibition of dendrite growth. Besides, the electric potential distributions in the y-direction and x-direction as illustrated in Fig. 7d and e reveal that the electric potential gradient is the highest in the y-direction under the combined electric field, resulting in the strongest electric field intensity. This enhances the migration of Li-ions in the y-direction, promoting more uniform lithium deposition and more effective dendrite suppression. In contrast, the electric potential distribution in the x-direction remains uniform, without significant increase in the potential gradient (see Fig. S8). Fig. 7f depicts the current density distribution in the y-direction. The results reveal that the current density is extremely uneven without an applied electric field. However, both the combined and individual electric fields effectively reduce local current density, promoting uniform lithium deposition and thereby suppressing dendrite growth in the y-direction.

To further investigate the impact of the combined electric field on dendrite suppression, we conducted a detailed study on how different DC voltages, AC voltages and AC frequencies inhibit dendrite growth. Fig. 7g illustrates the ratio of dendrite area with the combined electric field to that without any applied electric field across different DC voltages. The ratio initially decreases before increasing, reaching its minimum at a DC voltage of 0.1 V, which is consistent with the previously discussed optimal DC voltage for DCF. Fig. 7h presents the ratio of dendrite area under the combined electric field to that without any applied electric field at different AC voltages. The ratio increases with increasing AC voltages, with a 0.02 V AC voltage being proved to be the most effective in suppressing dendrite growth, aligning with the previously discussed optimal AC voltage. Fig. 7i shows the ratio of dendrite area with the combined electric field to that without any applied electric

field at different AC frequencies. It is evident that applying ACF perpendicular to the internal electric field provides better suppression effect than DCF, as illustrated in the dendrite area ratio of 14.01 % compared to 15.29 % for 25 Hz and 0 Hz, respectively. Further increase in the AC frequency gives rise to negligible variation of dendrite ratio. Therefore, a field frequency 25 Hz is identified as the optimal AC frequency, which is consistent with the previously discussed optimal AC frequency.

4. Conclusions

In summary, a comprehensive numerical investigation was conducted to assess the impact of superimposed ACF/DCF on the suppression of lithium dendrite formation in lithium metal batteries. Utilizing theoretical modeling and numerical simulation, distributions of the phase field, electric field, current density, and Li-ion concentration were analyzed to elucidate the underlying mechanisms governing lithium dendrite inhibition in the presence of external AC and DC fields. The application of ACF/DCF perpendicular to the internal electric field direction significantly suppressed dendrite growth, attributed to the markedly enhanced diffusion rate of Li-ions driven by the distortion of electric field distributions. This distortion attenuated the concentration gradient and local current density around the anode surface. Notably, the frequency-dependent variation of electric field directions in ACF further facilitated the homogeneous diffusion of Li-ions, leading to a reduction in dendrite area to only 15.75 % of that observed without an external electric field, under a voltage of 0.02 V and a frequency of 25 Hz. Similar dendrite suppression phenomena were observed when ACF/DCF was applied parallel to the internal electric field direction. This effect was primarily ascribed to the accelerated diffusion and migration of Li-ions along the field lines, which were enhanced by the strengthened electric field. Consequently, this configuration reduced the local current density in the y-direction and promoted more uniform Li-ion deposition, effectively inhibiting dendrite growth. The consistent electric field direction generated by DCF facilitated continuous and stable electric field enhancement. Thus, the application of external DCF parallel to the internal electric field proved to be more advantageous than that of ACF, resulting in a dendrite area of 15.18 % at a DC voltage of 0.1 V, compared to the condition without an external electric field. Remarkably, the simultaneous application of superimposed ACF and DCF yielded the optimal dendrite inhibition effect, exhibiting a dendrite area even smaller than that observed under either ACF or DCF alone. Overall, this study provides robust theoretical support for the implementation of external electric fields in suppressing lithium dendrite formation, which is crucial for addressing challenges associated with lithium dendrite growth and enhancing the performance and safety of lithium metal batteries. Future research will concentrate on the development of advanced numerical models and experimental studies to optimize ACF/DCF conditions across various battery operating scenarios, aiming to further validate the feasibility of utilizing external electric fields to inhibit dendrite formation in practical lithium metal battery applications.

CRediT authorship contribution statement

Huan Wang: Investigation, Formal analysis, Data curation, Conceptualization. **Daqian Wang:** Investigation, Data curation. **Hao Jiang:** Investigation. **Xiaolei Chen:** Investigation. **Xiaomin Liu:** Writing – review & editing, Supervision. **Bing Sun:** Writing – review & editing, Supervision, Investigation. **Yan Wang:** Writing – original draft, Supervision, Methodology, Investigation, Conceptualization.

Declaration of competing interest

The authors declare that they have no known competing financial interests or personal relationships that could have appeared to influence the work reported in this paper.

Acknowledgements

Y. Wang would acknowledge financial support from the Natural Science Foundation of Shandong Province (ZR2023MB131). B. Sun would like to thank the financial support from Australian Research Council through the ARC Future Fellowship (FT220100561).

Appendix A. Supplementary data

Supplementary data to this article can be found online at https://doi.org/10.1016/j.jpowsour.2025.236721.

Data availability

Data will be made available on request.

References

[1] M. Armand, J.M. Tarascon, Building better batteries, Nature 451 (7179) (2008) 652–657.
[2] P.R. Shearing, L.R. Johnson, Toward practical demonstration of high-energy-density batteries, Joule 4 (7) (2020) 1359–1361.
[3] Y. Zhang, C. Wei, M.-X. Wu, et al., A high-performance COF-based aqueous zinc-bromine battery, Chem. Eng. J 451 (2023) 138915.
[4] R. Dash, S. Pannala, Theoretical limits of energy density in silicon-carbon composite anode based lithium ion batteries, Sci. Rep. 6 (1) (2016) 27449.
[5] J. Wang, L. Chen, H. Li, et al., Anode interfacial issues in solid-state Li batteries: mechanistic understanding and mitigating strategies, Energy Environ. Mater. 6 (4) (2023) e12613.
[6] N. Xu, Y. Sun, J. Shi, et al., Fluorinated cyclic siloxane additives for high energy density Li-ion batteries with high nickel cathodes and silicon–carbon anodes, J. Power Sources 511 (2021) 230437.
[7] B. Horstmann, J. Shi, R. Amine, et al., Strategies towards enabling lithium metal in batteries: interphases and electrodes, Energy Environ. Sci. 14 (10) (2021) 5289–5314.
[8] Q.-H. Li, X.-F. Wang, S.-Y. Zhu, et al., Fast Li-ion conduction enabled by graphite fluoride flakes in solid polymer electrolyte, Rare Met. 42 (10) (2023) 3337–3344.
[9] J.-L. Liao, S. Zhang, T.-S. Bai, et al., A ZnO decorated 3D copper foam as a lithiophilic host to construct composite lithium metal anodes for Li–O2 batteries, Rare Met. 42 (6) (2023) 1969–1982.
[10] T. Lyu, F. Luo, D. Wang, et al., Carbon/lithium composite anode for advanced lithium metal batteries: design, progress, in situ characterization, and perspectives, Adv. Energy Mater. 12 (36) (2022) 2201493.
[11] B. Jagger, M. Pasta, Solid electrolyte interphases in lithium metal batteries, Joule 7 (10) (2023) 2228–2244.
[12] K. Shen, D. Wang, X. Ma, et al., In situ artificial solid electrolyte interface engineering on an anode for prolonging the cycle life of lithium-metal batteries, Dalton Trans. 52 (11) (2023) 3351–3357.
[13] S.-Y. Sun, X.-Q. Zhang, Y.-N. Wang, et al., Understanding the transport mechanism of lithium ions in solid-electrolyte interphase in lithium metal batteries with liquid electrolytes, Mater. Today 77 (2024) 39–65.
[14] Y. Chen, Y. Jiang, S.-S. Chi, et al., Understanding the lithium dendrites growth in garnet-based solid-state lithium metal batteries, J. Power Sources 521 (2022) 230921.
[15] Y. Huang, H. Yang, Y. Gao, et al., Mechanism and solutions of lithium dendrite growth in lithium metal batteries, Mater. Chem. Front. 8 (5) (2024) 1282–1299.
[16] S. Liu, N. Li, Y. Tang, et al., Mechanism of lithium dendrite growth on iron surfaces toward high-performance and safe anode-free lithium metal batteries, J. Mater. Chem. A 12 (16) (2024) 9886–9895.
[17] R. Jia, H. Dai, X. Tu, et al., Hexabutylcyclohexane-1,2,3,4,5,6-hexaimine additive-assisted commercial ester electrolyte for 4.7 V highly-stable Li-metal batteries, Adv. Energy Mater. 13 (47) (2023) 2302747.
[18] A. Wang, Y. Song, Z. Zhao, et al., Solvation engineering enables high-voltage lithium ion and metal batteries operating under −50 and 80 °C, Adv. Funct. Mater. 33 (35) (2023) 2302503.
[19] Y. Zhao, Z. Hu, Z. Zhao, et al., Strong solvent and dual lithium salts enable fast-charging lithium-ion batteries operating from −78 to 60 °C, J. Am. Chem. Soc. 145 (40) (2023) 22184–22193.
[20] W. Cao, Q. Li, X. Yu, et al., Controlling Li deposition below the interface, eScience 2 (1) (2022) 47–78.
[21] G. Lu, J. Nai, D. Luan, et al., Surface engineering toward stable lithium metal anodes, Sci. Adv. 9(14) eadf1550.
[22] C. Ma, X. Zhang, C. Liu, et al., Nano silica aerogel-induced formation of an organic/alloy biphasic interfacial layer enables construction of stable high-energy lithium metal batteries, Green Energy Environ. 8 (4) (2023) 1071–1080.
[23] W. Kou, Y. Zhang, W. Wu, et al., Thin polymer electrolyte with MXene functional layer for uniform Li+ deposition in all-solid-state lithium battery, Green Energy Environ. 9 (1) (2024) 71–80.

[24] Y.-T. Lv, T.-F. Zhang, Z.-T. Hu, et al., High critical current density in Li6.4La3Zr1.4Ta0.6O12 electrolyte via interfacial engineering with complex hydride, Rare Met. 43 (2) (2024) 692–701.
[25] S. Wang, Y. Liao, S. Li, et al., Ultrathin all-inorganic halide solid-state electrolyte membranes for all-solid-state Li-ion batteries, Adv. Energy Mater. 14 (6) (2024) 2303641.
[26] D. Huang, C. Zeng, M. Liu, et al., Introducing KI as a functional electrolyte additive to stabilize Li metal anode, Chem. Eng. J. 454 (2023) 140395.
[27] S. Sun, J. Yu, X. Ma, et al., In situ electrochemical polymerization of cathode electrolyte interphase enabling high-performance lithium metal batteries, Small (2024) 2403145.
[28] J. Zheng, W. Zhang, C. Huang, et al., In-situ polymerization with dual-function electrolyte additive toward future lithium metal batteries, Mater. Today Energy 26 (2022) 100984.
[29] H. Cheng, R. Tan, J. Li, et al., Coatings on lithium battery separators: a strategy to inhibit lithium dendrites growth, Molecules (2023).
[30] Y. Zhang, G. Zheng, Z. Yuan, et al., Review on interfacial compatibility of solid-state lithium batteries, Ionics 29 (5) (2023) 1639–1666.
[31] B.A. Budiman, A. Saputro, S. Rahardian, et al., Mechanical damages in solid electrolyte battery due to electrode volume changes, J. Energy Storage 52 (2022) 104810.
[32] S. Hong, K.H. Shin, S. Kim, et al., Mechanical-stress-Induced lithiation and structural evolution driven by excess lithium predisposing short circuits at the surface of garnet solid electrolytes, Adv. Energy Mater. (2024) 2402666.
[33] A. Van der Ven, R.M. McMeeking, R.J. Clément, et al., Ferroelastic toughening: can it solve the mechanics challenges of solid electrolytes? Curr. Opin. Solid State Mater. Sci. 27 (2) (2023) 101056.
[34] A. Wang, L. Zhang, J. Cao, et al., External field regulation of Li deposition in lithium metal batteries, Mater. Today Energy 42 (2024) 101557.
[35] J. Yao, G. Zhu, K. Dong, et al., Progress and perspective of controlling Li dendrites growth in all-solid-state Li metal batteries via external physical fields, Adv. Energy Sustainability Res. 5 (1) (2024) 2300165.
[36] K. Shen, Z. Wang, X. Bi, et al., Magnetic field–suppressed lithium dendrite growth for stable lithium-metal batteries, Adv. Energy Mater. 9 (20) (2019) 1900260.
[37] Y. Chen, X. Dou, K. Wang, et al., Lithium dendrites inhibition via diffusion enhancement, Adv. Energy Mater. 9 (17) (2019) 1900019.
[38] L. Gao, Z. Guo, Phase-field simulation of Li dendrites with multiple parameters influence, Comput. Mater. Sci. 183 (2020) 109919.
[39] W. Mu, X. Liu, Z. Wen, et al., Numerical simulation of the factors affecting the growth of lithium dendrites, J. Energy Storage 26 (2019) 100921.
[40] C. Zhang, D. Wang, C. Lei, et al., Effect of major factors on lithium dendrite growth studied by phase field modeling, J. Electrochem. Soc. 170 (5) (2023) 052506.
[41] G. Qi, X. Liu, R. Dou, et al., A three-dimensional multiphysics field coupled phase field model for lithium dendrite growth, J. Energy Storage 101 (2024) 113899.
[42] H. Chen, C. Lin, S. Li, et al., Improving lithium deposition in porous electrodes: phase field simulation, J. Energy Storage 95 (2024) 112606.
[43] L. Wang, S. Yao, C. Ying, et al., Numerical simulation of factors in charge of dendrite growth in zinc-nickel single flow batteries, Electrochim. Acta 475 (2024) 143622.
[44] L. Chen, H.W. Zhang, L.Y. Liang, et al., Modulation of dendritic patterns during electrodeposition: a nonlinear phase-field model, J. Power Sources 300 (2015) 376–385.
[45] V. Yurkiv, T. Foroozan, A. Ramasubramanian, et al., Phase-field modeling of solid electrolyte interface (SEI) influence on Li dendritic behavior, Electrochim. Acta 265 (2018) 609–619.
[46] R. Zhang, X. Shen, X.-B. Cheng, et al., The dendrite growth in 3D structured lithium metal anodes: electron or ion transfer limitation? Energy Storage Mater. 23 (2019) 556–565.
[47] Y. Li, L. Sha, G. Zhang, et al., Phase-field simulation tending to depict practical electrodeposition process in lithium-based batteries, Chin. Chem. Lett. 34 (2) (2023) 107993.
[48] K. Wang, P. Pei, Z. Ma, et al., Dendrite growth in the recharging process of zinc–air batteries, J. Mater. Chem. A 3 (45) (2015) 22648–22655.
[49] H. Zhao, C. Liao, C. Zhang, et al., Phase-field modeling of lithium dendrite deposition process: when an internal short circuit occurs, J. Energy Storage 100 (2024) 113779.
[50] D. Han, C. Lin, Numerical study of the formation of dead lithium during cycling and the mechanism of its effect on battery performance, J. Energy Storage 83 (2024) 110641.
[51] M.W. Verbrugge, B.J. Koch, Microelectrode study of the lithium/propylene carbonate interface: temperature and concentration dependence of physicochemical parameters, J. Electrochem. Soc. 141 (11) (1994) 3053.
[52] M.E. Arguello, N.A. Labanda, V.M. Calo, et al., Three-dimensional experimental-scale phase-field modeling of dendrite formation in rechargeable lithium-metal batteries, J. Energy Storage 62 (2023) 106854.